Microfluidic Platform to Study Intercellular Connectivity Through On-chip Electrical Impedance Measurement

Joel Dungan[1], Juanita Mathews[2], Michael Levin[2], Valencia Koomson[1]
Department of Electrical and Computer Engineering, Tufts University, Medford, MA 02155[1]
Department of Biology, Tufts University, Medford, MA 02155[2]

***Abstract*—A platform has been developed to study intercellular communication in non-neural cells as it relates to developmental biology and morphogenetic bioengineering. The versatile platform uses laminar flow in a microfluidic channel to create a "sucrose gap" that forces electrical signaling through a cell monolayer. The intercellular communication in the cell network is detected through electrical impedance measurements. A phase sensitive homodyne system has been designed and simulated in a 130nm CMOS process to provide a readout of cell monolayer complex impedance within the device. The system exhibits a highly linear conversion rate of 0.589mV/kΩ for cell layer impedances up to 1 MΩ.**

Keywords—CMOS; homodyne; lab-on-a-chip; gap junction

I. Introduction

Non-neural cells possess sophisticated intercellular communication mechanisms and are capable of forming networks and making decisions about cell growth and proliferation [1]. Non-neural cellular communication is mediated by gap junctions. These close cytosolic couplings allow the exchange of signaling molecules or ions between adjacent cells. Gap junctions are comprised of membrane proteins that can allow diffusion with high specificity [1-3]. Recent results have shown that connectivity between non-neural cells plays a crucial role in shaping cell development.

Patterns in connectivity established at the cellular level cascade into complex behaviors important to regenerative medicine and morphogenetic bioengineering. Altering gap junction activity has been shown to affect pattern formation [4], asymmetry [5], and organ growth, going so far as to induce the formation of multiple heads in planarians [6]. Errors in gap junction signaling can also cause abnormal growth that manifests as various disease states in humans, including forms of cancer [7]. Numerous studies have linked abnormal gap junction communication with tumor formation and carcinogenesis, and therapies focusing on gap junction regulation have met with some success in mouse models [8]. Gap junction-mediated signaling has been shown to affect the differentiation of multipotent cells [9], and in general, regulation of these electrical synapses is an essential component of exploiting developmental bioelectricity for the bioengineering of artificial living constructs (synthetic morphology) [10-12].

This work sponsored in part by the NSF IGERT program.

Traditionally, gap junction activity is examined via either the patch clamping method [13] or by observation of specialized diffusive dyes [9-11]. Whole cell patch clamping measures gap junction activity by recording the flow of charged ions through a cell membrane as an electrical voltage. However, the technique disrupts the membrane and is both expensive and technically challenging to perform, especially on more than a single cell. Dye diffusion methods attach fluorescent indicators to track the flow of signaling molecules through gap junctions. However, the results of these dye tests are difficult to quantify and repeatability is a significant issue.

To overcome the limitations of the existing technologies, a microfluidic platform is proposed to perform repeatable non-invasive assays on tissue networks. In a manner analogous to sucrose bridge experiments [14], the microfluidic chip electrically isolates a living cell culture, allowing precise impedance measurements that correspond to the average connectivity across the cells. This real time monitoring of cellular connectivity allows closed loop drug delivery studies that will test training and anticipation in gap junction networks. The ability to sense and manipulate gap junctional communication could have profound impacts on research and applications in developmental biology and tissue engineering.

II. Microfluidic Platform

A. Microfluidic Design

A microfluidic device that miniaturizes sucrose bridge experiments was presented in [15]. This work extends those results and incorporates key improvements to realize a true lab-on-chip research platform. The device takes advantage of the

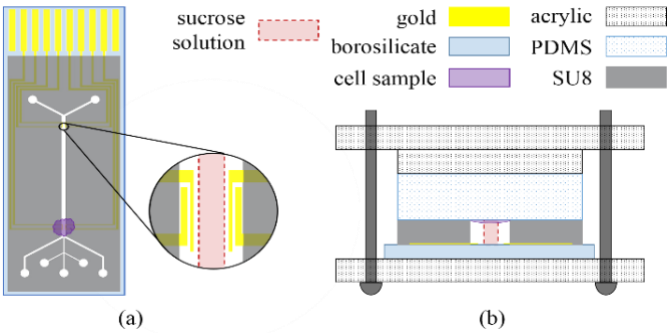

Fig. 1. (a) Topview of the microfluidic device, fluid inlets are on the bottom, pads at the top fit a standard card edge connector, (b) chip cross-section.

phenomenon of laminar flow to create three distinct fluid regions in a central channel, shown in Fig. 1. A sucrose based center stream creates a high impedance barrier which forces the majority of electrical signaling through the cell layer above. Thus, any current stimulus driven between the conductive saline side streams traverses the cell monolayer producing a recordable voltage that represents the average electrical impedance across the cell network.

Digitally controlled solenoid valves allow quick switching (on order of milliseconds) of the central stream among three high resistivity sucrose solutions, each which may be perfused with chemicals agents that induce changes in cell connectivity. This rapid automated solution exchange enables closed loop drug delivery experiments, in which drug delivery is modulated directly in response to electrical measurement of cellular network connectivity.

A polymethylsiloxane (PDMS) layer forming the top layer of the microchannels offers several advantages. Importantly, the device is much less susceptible to leaking because the elastomer accommodates some non-uniformity in the SU8 film. In addition to easing fabrication tolerances, the PDMS also allows trapped bubbles to outgas over time. Cell adhesion to PDMS has proved exceptional. In the case of normal rat kidney cells, adhesion to PDMS appears superior to glass and has been successfully demonstrated under laminar flow conditions for 24 hours.

B. Fabrication

The microfluidic chip, as diagrammed in Fig. 1, has been fabricated in the Tufts Micro/Nanofab. Cr/Au electrodes were patterned onto a borosilicate substrate using a liftoff process. The walls of the microfluidic channels were formed using MicroChem SU8-3050 at a thickness of 65um. A flat layer of PDMS (Sylgard 184), mixed at a ratio of 5:1 elastomeric base to curing agent in order to increase rigidity, forms the top of the microfluidic channels and serves as a substrate for cell culture. The layers of the device are compressed together in a custom housing laser cut from clear acrylic (ePlastics 1/8"). The housing provides even pressure generated through 6 screws and is designed to the dimensions of a standard 90 mm petri dish so that it can be easily mounted on an inverted microscope.

C. Electrical Measurement

The device has also been reconfigured to improve the electrode design and electrical measurement scheme. An additional set of electrodes have been incorporated to create a built in control channel. The electrodes have also been routed (under protective photoresist) to a single edge of the chip where a good electrical contact can be made via a standard chip edge connector. The connector routes all signals into a custom printed circuit board that houses the proposed integrated circuit to perform electrical impedance measurements.

III. Integrated Circuit

A. System Architecture

In order to prevent electroplating of the gold electrodes, an alternating current stimulus with low peak current (<1μA) is used to probe the cell layer. Taking advantage of the modulated

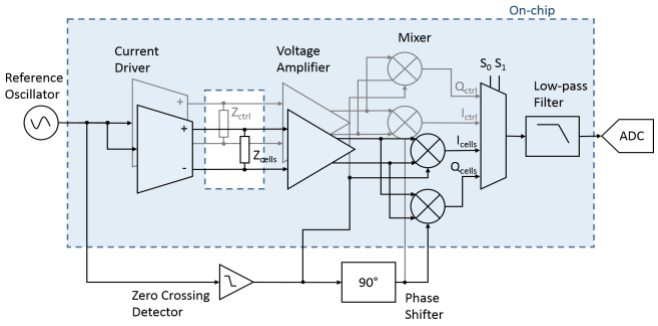

Fig. 2. System architecture.

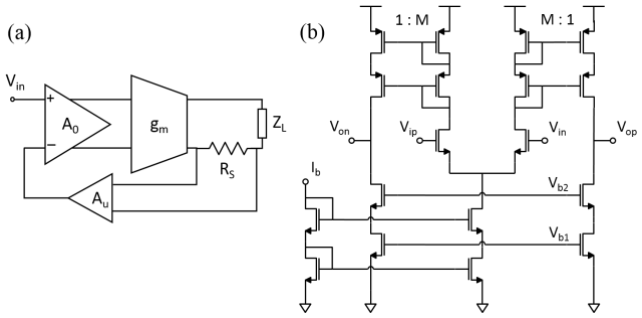

Fig. 3. (a) Feedback structure for differential current driver, (b) transistor level schematic of transconductance amplifier (biasing and CMFB not shown).

input, a homodyne demodulation scheme is proposed in Fig. 2 to both improve noise performance at the output and to function as a voltage readout circuit. Multiplying the voltage signal seen across the cell layer (Z_{cells}) by the original modulation frequency red-shifts the signal to 0 Hz, where a sharp ultra-low pass filter can significantly reduce the noise bandwidth. In addition to improving the SNR, the architecture of Fig. 1 enables phase sensitive detection for complex impedance measurement. In the quadrature channel, the signal is instead multiplied by a reference signal shifted by 90° relative to the reference, resulting in only the out of phase components of the signal appearing at output, Q_{cells}.

The architecture previously described is very similar to a "lock-in" amplifier, except that no phase-locked loop is employed to ensure that the I-channel is perfectly in phase. Integrated lock-in amplifiers have been presented previously [16-20], however, the chief difficulty in this design will result from high impedance loading. In preliminary measurements and previously published results [15], cell layer impedances have been measured in the range of hundreds of kilohms. Such high load impedances present considerable strain on the circuit stability and frequency response.

B. Current Driver

A highly stable precision AC current source is required for accurate measurements of absolute impedance in this system. If the waveform shape and frequency is provided by an external reference, as proposed, this current driver takes the form of a high precision transconductance amplifier. For this purpose many applications turn to the standard differential pair cell [21], [22]. However, the open loop transconductance of these cells cannot be easily guaranteed since it is a direct function of the input pairs' g_m values. Such designs are therefore very

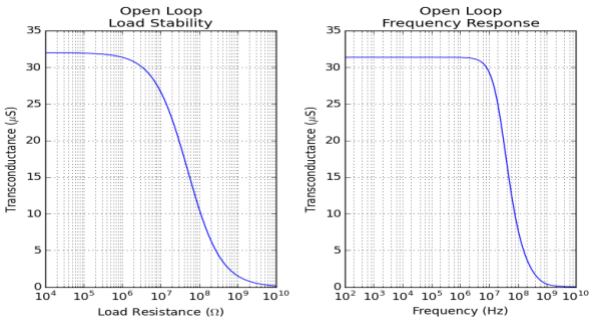

(a) (b)

Fig. 4. Simulation results for open loop transconductance amplifier.

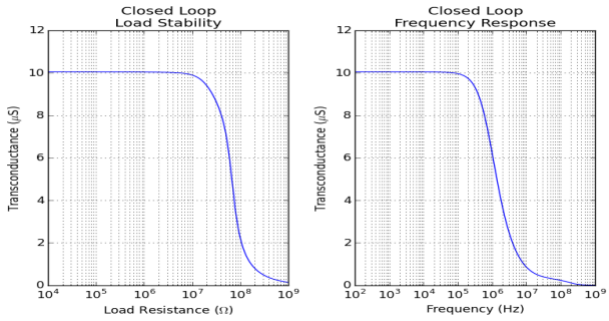

(a) (b)

Fig. 5. Simulation results for closed loop current driver.

susceptible to temperature changes, mismatch errors, and bias current fluctuations. In addition, in order to maintain stability over a large load impedance, the output impedance of the transconductor must be exceptionally high.

To establish a regulated transconductance and high output impedance, a feedback approach for a differential current driver is proposed [23], as shown in Fig. 3a. From two-port network theory, a transconductance amplifier with open-loop transconductance, G_m, that is connected through series-series feedback with a transimpedance amplifier of gain, R_f, will experience an enhanced closed loop transconductance, Γ_m, given by:

$$\Gamma_m = \frac{G_m}{1+G_m R_f}. \quad (1)$$

Similarly the output resistance, R_{out}, is also enhanced by the loop gain factor, $G_m R_f$:

$$R_{out} = r_0\left(1 + G_m R_f\right) \quad (2)$$

where r_0 is the output resistance of the original transconductor. In this structure, $G_m = A_0 g_m r_0/(r_0 + R_S + Z_L)$ and $R_f = A_u R_S$, such that from (1) the total transconductance can be approximated by

$$\Gamma_m \approx \frac{1}{A_u R_S} \quad (3)$$

when $r_0 \gg R_S + Z_L$ and $A_u A_0 g_m R_s \gg 1$. Letting $A_u = 1$, an R_S of 100 kΩ is chosen so that the driver can be directly controlled by a function generator or by the analog output port of a microcontroller producing a 100mV sinusoid signal.

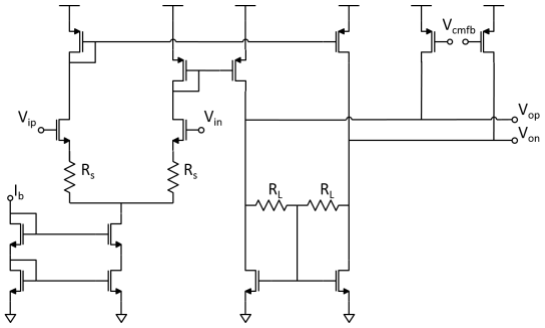

Fig. 6. Current feedback INA schematic (CMFB not shown).

The preamplifier (A_0) in Fig. 3a is implemented as a standard folded cascode amplifier with NMOS inputs. Miller compensation capacitors provide a feedforward path to bring the amplifier's phase margin to 55.03°. The open loop gain at low frequencies is greater than 68 dB.

Voltage to current conversion in the transconductor block (Fig. 3b) is achieved through a balanced differential pair. The resulting current is mirrored to the output at a ratio of M:1 via a double cascode mirror. A supply voltage of V_{dd}=3.3V provides ample headroom for this normally swing-expensive cascode mirroring structure. The mirror provides large output resistance by both reducing the output branch bias current by a factor of M and through capitalizing on the effects of cascoding. As demonstrated in Fig. 4a, where a resistive load is swept against a low frequency voltage input, the transconductor achieves an output resistance of 49 MΩ (i.e. where the transconductance falls by half). The frequency response of the transconductor under a 1 MΩ-2 pF load is presented in Fig 4b, showing that the output falls by 3dB at 26.3 MHz.

Transimpedance feedback is achieved through a unity gain buffer that senses the current flowing through sense resistor, R_S. The buffer is implemented with a differential difference amplifier (DDA) configured to shift the single ended output to $V_{dd}/2$ [24], [25].

The simulated output of the full feedback structure of Fig. 3 is shown in Fig. 5. The transconductance is regulated to 10 μS as expected for R_S = 100 kΩ. The driver exhibits good load stability with 0.05% transconductance variation over the expected operating range (100 kΩ < Z_L< 1 MΩ). The driver is gain stable up to a frequency of 110 kHz.

C. Demodulation Circuit

The instrumentation amplifier (INA) responsible for detecting the induced voltage difference across the cell layer is based on the current feedback topology presented in Fig. 6 [26]. The gain of this circuit is approximately R_L/R_S. Differential voltage at the input is converted to current through source degeneration resistors, R_S, in the first transconductor stage. In the second transimpedance amplifier stage, differential current flows through R_L, converting the signal back to voltage. Very high input impedance and a moderate gain of 2 are achieved in this system block.

The signal buffered by the INA is mixed with the square wave reference signal by a passive mixer, in which transmission gates reverse the polarity of the differential signal when the

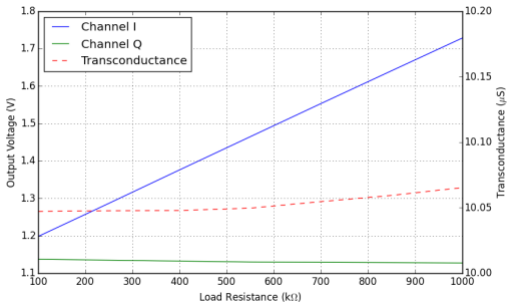

Fig. 7. Readout voltage of in-phase and out-of-phase channels of the full integrated circuit as the load resistance is swept of the physiologically relevant range.

reference signal is low. A difference amplifier converts the output to a single ended voltage for filtering. For the purposes of the simulation results presented in Fig. 7, a simple passive third order RC filter has been used.

IV. Results

Fig. 7 shows the simulated response of the integrated impedance measurement circuit. As the load resistance of the cells is swept across the physiologically relevant range, the system exhibits a highly linear response with a conversion rate of 0.589 mV/kΩ ($R^2 > 0.999$), while the current driver remains stable. The Q-channel readout remains constant over a resistive load sweep. Further work aims to complete the integration of an OTA-C architecture for the final low pass filter element. Upon fabrication, the proposed integrated circuit will enable precise electrical measurement of gap junction mediated cellular interconnectivity in a lab-on-a-chip device, ideal for investigation of in vitro models of regenerative biology and physiological plasticity [27], [28].

References

[1] J. Mathews and M. Levin, "Gap junctional signaling in pattern regulation: Physiological network connectivity instructs growth and form.," Developmental Neurobiology, Jun. 2016.

[2] E. Scemes, S. Suadicani, G. Dahl, and D. Spray, "Connexin and pannexin mediated cell-cell communication," Neuron Glia Biology, vol. 3, no. 3, pp. 199–208, Nov. 2008.

[3] G. Sohl and K. Willecke, "Gap junctions and the connexin protein family," Cardiovascular Research, vol. 62, no. 2, pp. 228–232, May 2004.

[4] K. J. Sims, D. Eble, and M. Iovine, "Connexin43 regulates joint location in zebrafish fins," Development Biology, vol. 327, no. 2, pp. 410–418, Mar. 2009.

[5] C.-F. Chuang, M. K. VanHoven, R. D. Fetter, V. K. Verselis, and C. I. Bargmann, "An innexin-dependent cell network establishes left-right neuronal asymmetry in C. elegans," Cell, vol. 129, no. 4, pp. 787–799, May 2007.

[6] M. Emmons-Bell et al., "Gap junctional blockade stochastically induces different species-specific head anatomies in genetically wild-type Girardia dorotocephala flatworms," International Journal of Molecular Sciences, vol. 16, no. 11, pp. 27865–27896, Nov. 2015.

[7] Y. Omori and H. Yamasaki, "Mutated connexin43 proteins inhibit rat glioma cell growth suppression mediated by wild-type connexin43 in a dominant-negative manner.," International Journal of Cancer, vol. 78, no. 4, pp. 446–453, Nov. 1998.

[8] B. Chernet, C. Fields, and M. Levin, "Long-range gap junctional signaling controls oncogene-mediated tumorigenesis in Xenopus laevis embryos," Frontiers in Physiology, vol. 5, p. 519, Jan. 2015.

[9] N. Oviedo and M. Levin, "smedinx-11 is a planarian stem cell gap junction gene required for regeneration and homeostasis," Development, vol. 134, pp. 3121–3131, Aug. 2007.

[10] M. Levin, G. Pezzulo, and J. M. Finkelstein, "Endogenous Bioelectric Signaling Networks: Exploiting Voltage Gradients for Control of Growth and Form," Annual Review of Biomedical Engineering, vol. 19, in press.

[11] M. Levin, "Molecular bioelectricity: how endogenous voltage potentials control cell behavior and instruct pattern regulation in vivo," Molecular Biology of the Cell, vol. 25, no. 24, pp. 3835–3850, Dec. 2014.

[12] M. Levin, "Reprogramming cells and tissue patterning via bioelectrical pathways: molecular mechanisms and biomedical opportunities," WIREs Systems Biology and Medicine, vol. 5, no. 6, pp. 657–676, Jul. 2013.

[13] A. D. G. de Roos, E. J. J. van Zoelen, and A. P. R. Theuvenet, "Determination of gap junctional intercellular communication by capacitance measurements," Pflugers Arch., no. 431, pp. 556–563, 1996.

[14] T. Mert, "Sucrose-gap technique: Advantages and limitations," Neurophysiology, vol. 39, no. 3, pp. 270–274, May 2007.

[15] C. Bathany, D. L. Beahm, S. Besch, F. Sachs, and S. Z. Hua, "A microfluidic platform for measuring electrical activity across cells," Biomicrofluidics, vol. 6, no. 3, Sep. 2012.

[16] F. Badets, J.-G. Coutard, P. Russo, E. Dina, E. Gliere, and S. Nicoletti, "A 1.3 mW, 12-bit lock-in amplifier based readout circuit dedicated to photo-acoustic gas sensing," presented at the SENSORS, 2016.

[17] A. De Marcellis, G. Ferri, and A. D'Amico, "One-decade frequency range, in-phase auto-aligned 1.8 V 2 mW fully analog CMOS integrated lock-in amplifier for small/noisy signal detection," IEEE Sensors Journal, vol. 16, no. 14, pp. 5690–5701, May 2016.

[18] P. M. Maya-Hernandez, M. T. Sanz-Pascual, and B. Calvo, "Micropower CMOS lock-in amplifier for portable applications," Electronics Letters, vol. 52, no. 10, pp. 828–830, May 2016.

[19] C. Qi, Y. Huang, W. Zhang, D. Zhou, Y. Wang, and M. Zhu, "Design of dual-phase lock-in amplifier used for weak signal detection," presented at the Industrial Electronics Society Annual Conference, 2016.

[20] J. Xu, G. Meynants, and P. Merken, "Low-power lock-in amplifier for complex impedance measurement," presented at the 3rd International Workshop on Advances in Sensors and Interfaces, 2009, pp. 1–5.

[21] H. Hong, M. Rahal, A. Demosthenous, and R. H. Bayford, "Comparison of a new integrated current source with the modified Howland circuit for EIT applications.," Physiological Measurement, vol. 30, no. 10, pp. 999–1007, Aug. 2009.

[22] S. Hong et al., "A 4.9 mΩ-Sensitivity mobile electrical impedance tomography IC for early breast-cancer detection system," IEEE Journal of Solid-State Circuits, vol. 50, no. 1, pp. 245–257, Sep. 2014.

[23] L. Constantinou, I. F. Triantis, R. Bayford, and A. Demosthenous, "High-power CMOS current driver with accurate transconductance for electrical impedance tomography," IEEE Transactions on Biomedical Circuits and Systems, vol. 8, no. 4, pp. 575–583, Jan. 2014.

[24] S.-C. Huang, M. Ismail, and S. R. Zarabadi, "A wide range differential difference amplifier: a basic block for analog signal processing in MOS technology," IEEE Transactions on Circuits and Systems II: Analog and Digital Signal Processing, vol. 40, no. 5, pp. 289–301, Aug. 2002.

[25] E. Sackinger and W. Guggenbuhl, "A versatile building block: the CMOS differential difference amplifier," IEEE Journal of Solid-State Circuits, vol. 22, no. 2, pp. 287–294, Jan. 2003.

[26] V. Valente and A. Demosthenous, "Wideband fully-programmable dual-mode CMOS analogue front-end for electrical impedance spectroscopy," Sensors, vol. 16, no. 8, p. 1159, Jul. 2016.

[27] G. Pezzulo and M. Levin, "Top-down Models in biology: Explanation and control of complex living systems above the molecular level," Journal of the Royal Society Interface, vol. 13, no. 124, Nov. 2106.

[28] K. Sullivan, M. Emmons-Bell, and M. Levin, "Physiological inputs regulate species-specific anatomy during embryogenesis and regeneration," Communicative and Integrative Biology, vol. 9, no. 4, p. e1192733, Jul. 2016.